


Article

# Long-Term Modelling of an Agricultural and Urban River Catchment with SWMM Upgraded by the Evapotranspiration Model UrbanEVA

Frauke Kachholz \* and Jens Tränckner 

Department of Water Management, University of Rostock, Satower Straße 48, 18059 Rostock, Germany; jens.traenckner@uni-rostock.de

\* Correspondence: frauke.kachholz@uni-rostock.de

Received: 24 September 2020; Accepted: 2 November 2020; Published: 4 November 2020



**Abstract:** Evapotranspiration (ET) has a decisive effect on groundwater recharge and thus also affects the base flow of the receiving water. This applies above all to low-lying areas with a low depth to groundwater (GW), as is often the case in the north German lowlands. In order to analyze this relation, a coupled rainfall-runoff and hydraulic stream model was set up using the software SWMM-UrbanEVA, a version of the software SWMM that was upgraded by a detailed ET module. A corresponding model was set up for the same site but with the conventional software SWMM to compare the water balance and hydrographs. The total amount of ET calculated with the SWMM software is 7% higher than that computed with the upgraded version in the period considered. Therefore, less water is available for soil infiltration and lateral groundwater flow to the stream. This generally leads to a slight underestimation of base flows, with the exception of a notably wet summer month when the base flows were highly overestimated. Nevertheless, the base flow hydrograph shows a good adaptation to observed values ( $MAE = 0.014 \text{ m}^3\text{s}^{-1}$ ,  $R = 0.88$ ,  $NSE = 0.81$ ) but gives worse results compared to SWMM-UrbanEVA. The latter is very well able to reflect the GW-fed base flow in the sample stream in average ( $MAE = 0.011 \text{ m}^3\text{s}^{-1}$ ) and in its dynamics ( $R = 0.93$ ,  $NSE = 0.85$ ). By applying the UrbanEVA upgrade, SWMM is applicable to model the seasonal dynamics of near-natural river basins.

**Keywords:** storm water management model (SWMM); evapotranspiration; streamflow; hydrologic/hydraulic modelling; SWMM-UrbanEVA

## 1. Introduction

The storm water management model (SWMM) was originally developed for the simulation and evaluation of storm runoff and sewer hydraulics in urban areas [1]. Since the introduction of SWMM in 1971, it has been continuously improved and thus opens up more and more fields of application. One of the biggest advantages of SWMM is that it combines both a hydrological rainfall-runoff model with a hydrodynamic drainage model in one software. This makes the numerical calculation very effective and stable, as no external coupling is necessary. Besides the modelling of urban infrastructure, like pipes, pumps, flow dividers and storage units, etc., it also allows the modelling of open streams with natural cross sections. Furthermore, the rainfall runoff model enables reliable groundwater simulation, as it uses physical parameters to calculate storage and discharge. Comparable models, e.g., Hec-HMS, only represent the aquifer in a simplified way [2]. As versatile as SWMM is, it has one drawback. This consists in the fact that the latest SWMM version (5.1.015) calculates purely physical actual evaporation from different environmental compartments but does not account for the biological transpiration of plants. When simulating a single rain event, this is not relevant, since ET practically does not take place and therefore has no significant impact on discharges. Considering a long-term

simulation in a region, where the transpiration of plants accounts for a large part of the total ET, the components of the water balance, like soil infiltration and percolation to the GW zone, cannot be modelled accurately. In cross-season simulations, this leads to incorrect feed of storage systems and hence to systematic volume errors in the river flow.

Despite the simplified ET calculation, SWMM has been used more often in rural areas in recent years [3–7]. Due to its broad application, the desire for continuous improvement of SWMM is growing not only among the developers of the software but also among its users. For some research questions or applications, it is possible to use SWMM's existing components to improve model performance [8]. For the ET calculation of plants, the internal software tools are no longer sufficient, so that the source code must be adjusted. Regarding the implementation of a vegetation-specific ET this has been done successfully at the University of Utah, USA [9] and the University of Applied Sciences Münster, Germany [10]. The two use different approaches:

The authors of [9] allow the input of multiple time series of potential ET and additionally implement a water stress coefficient for the calculation of actual ET, which serves to reduce ET rates at low soil water contents. The comparison between simulated and measured actual ET rates showed that the updated ET routine works well for a bioretention site ( $R = 0.75$ ) and green roof ( $R = 0.88$ ). According to [9], the input of a “mismatched” (crop non-specific) potential ET time series can lead to an overestimation of 12–19% of annual actual ET and an underestimation of 14–19% of annual runoff.

The second approach [10–12] integrates a vegetation layer into SWMM's low impact development (LID) module and calculates actual interception and transpiration on the basis of one input time series for potential grass reference ET. In the process, a crop factor is implemented, which reflects the water demand of a plant and reduces or increases the ET rates depending on the vegetation type [13]. The upgraded SWMM version is called SWMM-UrbanEVA and has been developed in order to cope with the ET of vegetation at the micro- (green roof) to mesoscale (city district) [11]. By applying SWMM-UrbanEVA, the volume error of the runoff from a green roof could be improved from almost 17% to about 4% [12].

The present work tests the applicability of SWMM-UrbanEVA in the macroscale of a river catchment at the example of the Schmarler stream system in the north German lowlands. Results are compared with the results of the conventional SWMM software.

## 2. Materials and Methods

### 2.1. Study Area and Monitoring Station

The study area is the catchment of the Schmarler stream system, located in the north-eastern German lowlands. It is part of the city of Rostock and its rural surroundings (see Figure 1). The stream network altogether is 35 km long, consisting of open segments, pipes, and culverts. The main stream discharges into the river Warnow, which drains into the Baltic Sea. In total, 65% of the 23-km<sup>2</sup> catchment area is occupied by vegetation, while approximately 34% of the area is partial impervious, which is due to urban use (residential area, traffic area, and industry/trade; see Table 1). The annual average precipitation is 600–700 mm, of which 350–575 mm evapotranspires depending on the type of land use and water availability [14]. The topography is relatively flat, ranging from 29 to 0 m above mean sea level. In most parts of the area, the depth to GW is relatively low (<5 m), which causes a significant seasonal component of base flow in the river system.

In the area of the Schmarler stream station 2 + 400, a monitoring station for continuous measurement of water level and flow velocity was installed (see Figure 1) in order to calculate flow rates from the two parameters. To accomplish this, an ultrasonic doppler flow meter was used. Since the device only measures flow velocity in the central lamella, a calibration function based on regular comparative manual multi-point measurements was set-up to obtain the mean flow velocity of the complete cross section. Figure 2 shows the corrected data at the monitoring station “Autobahn” (AB). Due to random errors, the noise of the data is quite high. Therefore, the time series was smoothed using the 3-h moving median. The latter was processed to separate the base flows, based on the sliding interval method [15] by forming the minimum of 3-day periods, respectively (Figure 3).

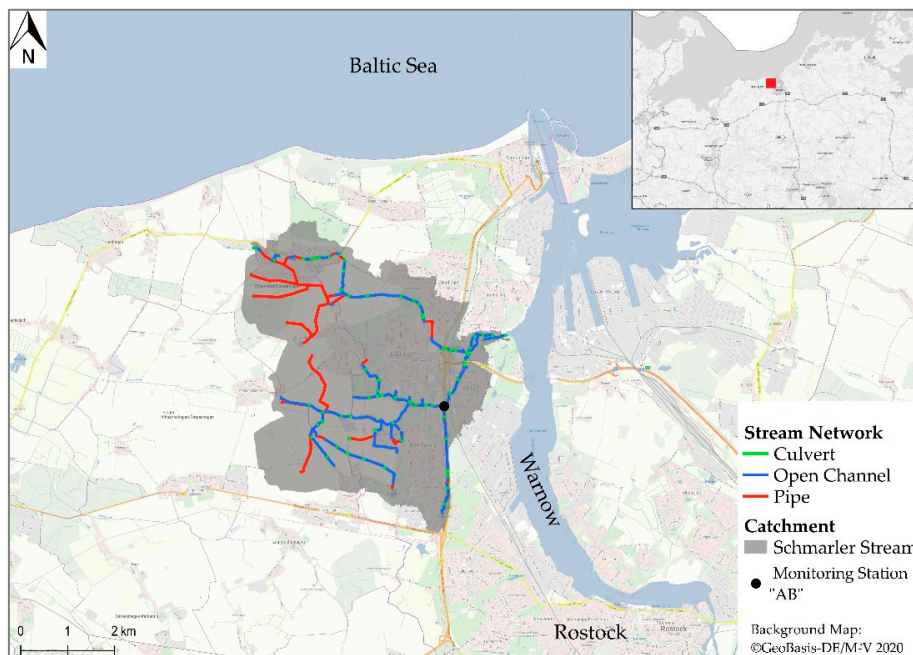


Figure 1. Schmarler stream system and catchment.

Table 1. Different types of land use and their area percentage in the Schmarler stream catchment.

Land Use Class	Abbreviation	Area Fraction (%)	Thereof Sealed (%)
agriculture	AC	29.2	0
wetland	WL	0.1	0
grassland	GL	1.3	0
industry/trade	IT	5.0	62.5
deciduous forest	DF	0.3	0
mixed forest	MF	6.0	0
coniferous forest	CF	1.3	0
orchard	OR	11.5	0
residential area	RA	17.8	49.4
parks	PA	15.3	26.7
traffic area	TA	11.0	51.0
water surface	WA	1.2	0

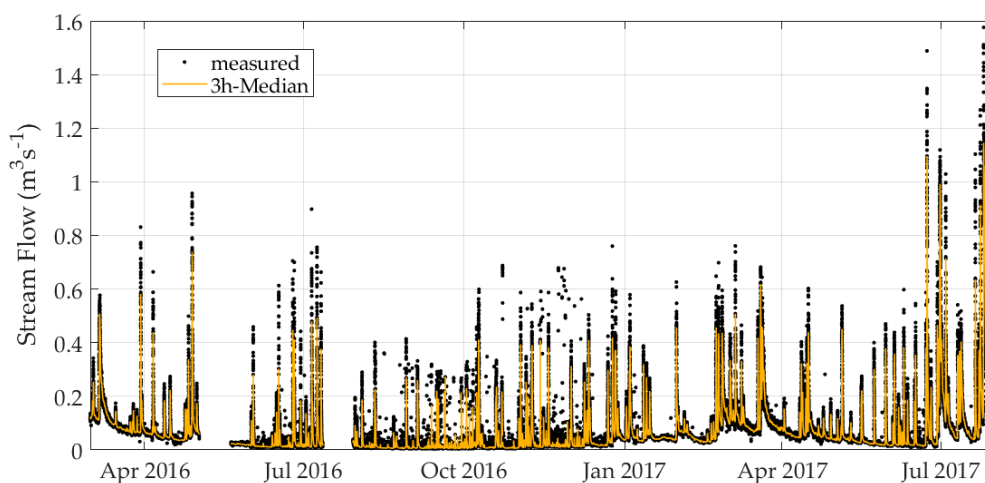
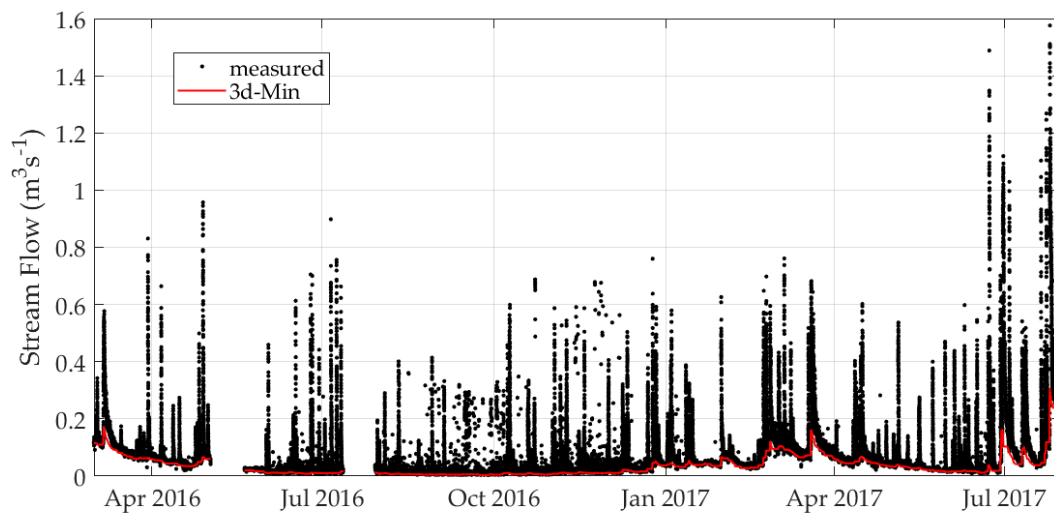


Figure 2. Measured stream flow and corresponding smoothed curve (3-h-median sliding interval) at the monitoring station “Autobahn” (AB).



**Figure 3.** Measured stream flow and 3-day-minimum (sliding interval) to represent base flow at the monitoring station “Autobahn” (AB).

## 2.2. Software Description

### 2.2.1. SWMM

The Storm Water Management Model SWMM is an open source software used for the simulation of the surface/subsurface runoff from primarily urban areas. It was developed by the United States Environmental Protection Agency (EPA) and combines a hydrological rainfall-runoff model with a hydrodynamic drainage model. The former traditionally consists of four compartments: (1) the atmosphere, (2) the land surface, (3) the sub-surface, and (4) the GW compartment. The rainfall-runoff model is semi-distributed and operates on a number of subcatchments consisting of permeable and impermeable sub-areas. Furthermore, SWMM’s version 5 introduces the low-impact development controls (LIDs), such as a bioretention cell or a green roof, used to calculate runoff, storage, and infiltration in a more detailed way [1,16]. Different calculation algorithms are available for the different compartments of the rainfall-runoff model; the ones used in this study are described below.

The atmosphere module contains time series for precipitation and  $ET_0$ . The latter can only be set globally for the entire model area while distinct precipitation time series can be defined for every subcatchment. Originally, evaporation can occur for standing water on subcatchment surfaces, for subsurface water in aquifers, for water held in storage units, and for open channel flow [1]. The land surface receives precipitation and generates surface runoff using the nonlinear reservoir routing method. For infiltration calculation in the sub-surface zone of the subcatchments, SWMM offers five optional methods. For this study, the Horton method was chosen. It assumes that the infiltration capacity is high at the beginning of a rain event (maximum infiltration rate) and then decreases exponentially with increasing water content in the soil until a state of equilibrium is reached (minimum infiltration rate). However, for infiltration within the LID, SWMM only offers the Green & Ampt Scheme. In SWMM, the aquifer can lose or transfer water respectively through deep percolation, ET, and lateral GW flow to the drainage network. The height of the water table varies with time depending on the rates of inflow and outflow. Lateral GW flow is represented through a user-defined power function of the changing water table of the aquifer and depth of water in the receiving node of the conveyance system [1]:

$$Q_{GW} = A1(H_{GW} - H_{CB})^{B1} - A2(H_{SW} - H_{CB})^{B2} + A3(H_{GW}H_{SW}), \quad (1)$$

$Q_{GW}$  = lateral groundwater flow ( $m^3s^{-1}ha^{-1}$ );

$H_{GW}$  = GW level above aquifer bottom (m);

$H_{CB}$  = height of channel bottom above aquifer bottom (m);  
 $H_{SW}$  = height of surface water at receiving node above aquifer bottom (m);  
 $H_{CB}$  = height of channel bottom above aquifer bottom (m);  
 $A1$  = groundwater flow coefficient ( $m^{(1-B1)}s^{-1}$ );  
 $B1$  = groundwater flow exponent (-);  
 $A2$  = surface water flow coefficient ( $m^{(1-B2)}s^{-1}$ );  
 $B2$  = surface water flow exponent (-); and  
 $A3$  = surface – groundwater interaction coefficient ( $(m - s)^{-1}$ ).

A threshold set by the user makes it possible to determine from which water level lateral GW flow to the stream network will occur [16,17]. This also enables the simulation of tile drainage.

The hydrodynamic drainage model is subdivided into nodes and conduits and receives its water from the subcatchments (runoff from surface and GW interflow) at defined nodes. The drainage network may consist of open sections, pipes, culverts, and other control structures like pumps and weirs. Gravity flow within the conduit link is calculated using the one-dimensional Saint–Venant equation, allowing different options (kinematic/diffuse/dynamic wave). Here, the dynamic wave option was applied, which enables the simulation of channel storage, backwater effects, and entrance/exit losses [17,18].

### 2.2.2. SWMM-UrbanEVA

As an upgrade of the original SWMM version, SWMM-UrbanEVA was developed at the University of Applied Sciences Münster (Germany) to calculate ET more precisely. It was designed as part of the well-known LID module (Figure 4) and contains an approach for calculating the actual ET of vegetated areas based on the potential grass reference ET ( $ET_0$ ). The existing three-layer system of the traditional LID module (surface-soil-storage) serves to model the infiltration and percolation processes depending on soil parameters. It is supplemented by a new vegetation layer in which vegetation-specific properties, like the crop factor ( $K_C$ ) [13] and the leaf area index (LAI), can be parameterized (Figure 4).

The actual vegetation-specific ET ( $E_{STI,a}$ ) is computed for every time step and comprises the sub processes of interception, transpiration, soil evaporation, and evaporation of free water surfaces:

$$E_{STI,a} = E_{I,a} + E_{T,a} + E_{S,a} + E_{W,a}, \quad (2)$$

$E_{I,a}$  = actual rate of interception ( $mmh^{-1}$ );  
 $E_{T,a}$  = actual rate of transpiration ( $mmh^{-1}$ );  
 $E_{S,a}$  = actual rate of soil evaporation ( $mmh^{-1}$ ); and  
 $E_{W,a}$  = actual rate of free water surface ( $mmh^{-1}$ ).

The calculation of each component is based on the potential vegetation-specific ET ( $E_{STI,p}$ ). The latter is obtained by multiplying  $K_C$  with the input  $ET_0$ :

$$E_{STI,p} = ET_0 \times K_C, \quad (3)$$

$E_{STI,p}$  = vegetation – specific potential ET ( $mmh^{-1}$ ); and  
 $ET_0$  = grass reference evapotranspiration ( $mmh^{-1}$ ).

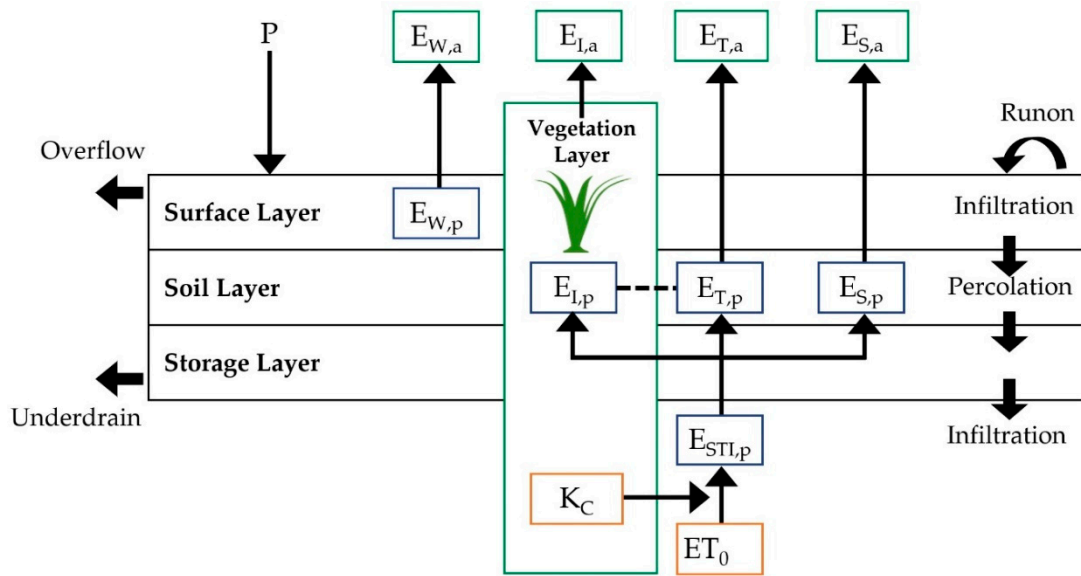


**Figure 4.** Components of evapotranspiration as part of the enhanced LID module of SWMM-UrbanEVA. (P = Precipitation,  $K_C$  = crop factor,  $ET_0$  = potential grass reference ET,  $E_{STL,p}$  = plant specific potential ET,  $E_{I,p}$  = pot. interception,  $E_{T,p}$  = pot. transpiration,  $E_{S,p}$  = pot. soil evaporation,  $E_{W,p}$  = pot. evaporation of free water surface,  $E_{W,a}$  = actual evaporation of free water surface,  $E_{I,a}$  = actual interception,  $E_{T,a}$  = actual transpiration,  $E_{S,a}$  = actual soil evaporation)—figure kindly provided by Birgitta Hörnschemeyer (modified).

Interception and transpiration are energetically decoupled from soil evaporation via the vegetation-covered fraction (SCF) of the surface [19,20].

The interception height ( $I$ ) is derived depending on the leaf area index according to the approach of [21]. The LAI reflects the ET-active surface in the annual cycle and determines the maximum storage capacity of the leaf canopy:

$$I = S_{max} \times \left( 1 - \frac{1}{1 + \frac{SCF \times P}{S_{max}}} \right), \quad (4)$$

$$SCF = 1 - 0.7^{LAI_{doy}}, \quad (5)$$

$$S_{max} = S_L \times LAI_{doy}, \quad (6)$$

$I$  = potetial interception height (mm);

$S_{max}$  = max. interception height (mm);

$S_L$  = leaf storage coefficient (mm), [11] recommends  $S_L = 0.29$  (mm);

$LAI_{doy}$  = LAI corresponding to day of year (-) (here monthly resolution);

$SCF$  = vegetation covered fraction (-); and

$P$  = precipitation (mm).

Interception occurs only from the wetted part of the leaf and is determined on the one hand by the precipitation height at low precipitation rates and on the other hand by the maximum interception capacity ( $S_{max}$ ) at high precipitation rates [21]. The potential interception height of the current time step  $i$  ( $S_i$ ) depends on the previous time step  $i-1$  ( $S_{i-1}$ ):

$$S_i = S_{i-1} + I. \quad (7)$$

The actual intercept height  $S_{I,a}$  is then derived depending on the interception capacity and the interception height of the current time step:

$$S_{I,a} = \begin{cases} S_I & \text{for } S_I \leq S_{max} \\ S_{max} & \text{for } S_I > S_{max} \end{cases} \quad (8)$$

To calculate the potential interception rate  $E_{I,p}$ , the potential evapotranspiration  $E_{STI,p}$  is reduced using the vegetation-covered fraction and the wetted part of the leaf  $A_b$  [22,23]:

$$E_{I,p} = SCF \times A_b \times E_{STI,p}, \quad (9)$$

in which:

$$A_b = \left( \frac{S_{I,a}}{S_{max}} \right)^{\frac{2}{3}}. \quad (10)$$

The actual interception rate  $E_{I,a}$  finally results from the minimum fill level of the interception height and the potential evaporation rate:

$$E_{I,a} = \min(S_{I,a}, E_{I,p}). \quad (11)$$

The part of the precipitation that does not intercept is returned to the input precipitation, which enters the following infiltration and drainage processes:

$$P_{net} = P \times (1 - SCF) + (P - E_{I,a}) \times SCF \quad (12)$$

$P_{net}$  = Precipitation subtracted by interception losses ( $\text{mmh}^{-1}$ ); and

$P$  = input precipitation ( $\text{mmh}^{-1}$ ).

Equivalent to the potential interception rate, the potential transpiration rate  $E_{T,p}$  is projected onto the vegetation-covered area. In contrast to interception, transpiration takes place from the dry portion of the leaf ( $1 - A_b$ ). Furthermore, the actual interception evaporation rate  $E_{I,a}$  is subtracted as an upstream process:

$$E_{T,p} = SCF \times (1 - A_b) \times E_{STI,p} - E_{I,a}. \quad (13)$$

Since the process of transpiration is fed from the soil reservoir, the calculation of the actual transpiration rate  $E_{T,a}$  is done in dependence of the available soil water:

$$E_{T,a} = \min \left( \frac{(\theta - \theta_{WP}) \times D}{\Delta t}, E_{T,p} \right), \quad (14)$$

$\theta$  = actual moisture content (-);

$\theta_{WP}$  = moisture content at wilting point(-);

$D$  = thickness of soil layer (mm); and

$\Delta t$  = simulation time step.

Soil evaporation is computed for the uncovered area share ( $1 - SCF$ ), as it is assumed that evaporation underneath vegetation is negligible [24]:

$$E_{S,p} = (1 - SCF) \times E_{STI,p} \quad (15)$$

$E_{S,p}$  = potential soil evaporation ( $\text{mmh}^{-1}$ ).

The actual soil evaporation depends on the water content of the soil and is expressed by the relative soil moisture  $W_{rel}$ . The latter describes the proportion of available soil water within the range of the usable field capacity:

$$W_{rel} = \frac{\theta - \theta_{WP}}{\theta_{FK} - \theta_{WP}}, \quad (16)$$

$W_{rel}$  = relative soil moisture (-); and  
 $\theta_{FK}$  = moisture content at field capacity (-).

According to [25], the potential evaporation rate is already met before the water content in the soil reaches field capacity. For this reason, the potential evaporation rate is increased by the coefficient  $e_s$  if the relative soil moisture falls below a certain threshold (see Equations (17) and (18)). According to the recommendations of [20,25], this threshold is set to 0.6:

$$e_s = \begin{cases} \left(\frac{W_{rel}}{0.6}\right)^{0.5} & \text{for } W_{rel} < 0.6 \\ 1 & \text{for } W_{rel} \geq 0.6 \end{cases}, \quad (17)$$

$$E_{S,p} = e_s \times E_{S,p}. \quad (18)$$

The actual soil evaporation  $E_{S,a}$  is finally calculated from the minimum of the available soil water per time step and the potential soil evaporation rate:

$$E_{S,a} = \min\left(\frac{(\theta - \theta_{WP}) \times D}{\Delta t}, E_{S,p}\right). \quad (19)$$

If ponding occurs, two options can be chosen: In the case that vegetation height is short and completely covered by ponding water, only evaporation from the free water surface occurs while the other ET processes are suspended:

$$E_{I,a} = 0, \quad (20)$$

$$E_{T,a} = 0, \quad (21)$$

$$E_{S,a} = 0, \quad (22)$$

$$E_{W,p} = E_{STI,p}, \quad (23)$$

$$E_{W,a} = \min\left(\frac{h_{pond}}{\Delta t}, E_{W,p}\right), \quad (24)$$

$h_{pond}$  = height of ponding surface water (mm).

In the case of a high stand, such as a forest, only soil evaporation stops while interception, transpiration and evaporation of the free water surface will continue.

### 2.3. Model Setup

Both the setup of the rainfall-runoff model and the setup of the stream model was realized on the basis of GIS data. VBA scripts were used to convert them to the text format used by SWMM. Water courses were provided as lines and marked with a hierarchical stream segment index, which enables the assignment of a stream segment to a subcatchment and vice versa. Stream cross sections were derived from a high-resolution digital elevation model (DEM) with a grid size of 0.2 m. Each subcatchment was shaped by intersecting the superficial subcatchments based on DEM analysis and land use polygons (Figure 5). Soil type maps were used to derive average soil attributes for each subcatchment and LID control while the aquifer was treated as homogeneous sand across the model area but with different fill levels depending on the average ground elevation of the subcatchments. GW flow to the river only occurs if a defined threshold is exceeded by the water table. Here, it is



1.2 m below the average ground height, as in the case of a drainage pipe, which comes on stream when the surrounding soil is saturated. The unsealed area of a subcatchment was simulated using the LID controls, more precisely a bioretention cell with the upgraded ET calculation. Furthermore, an equal model was set up for comparison with the same LID controls but with the conventional evaporation calculation.

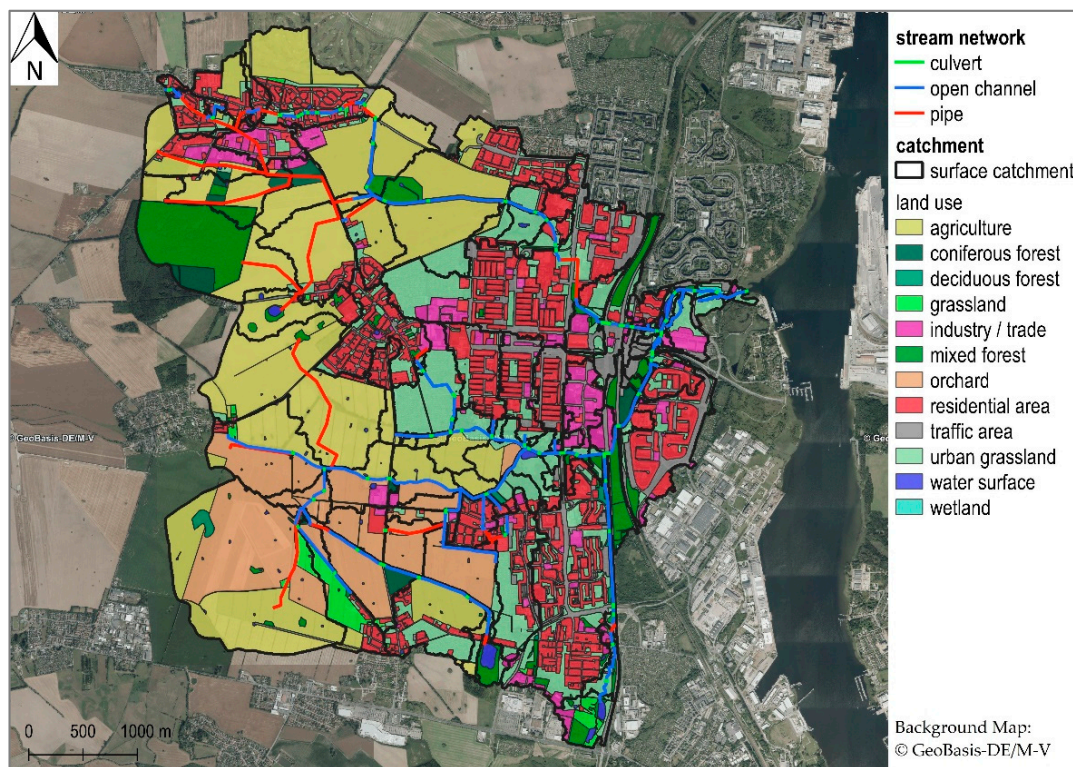


**Figure 5.** Model subcatchments as intersection of the surface catchments and land use polygons.

Important additional input parameters for SWMM-UrbanEVA are the crop factor and the leaf area index with its annual cycle (Figure 6). In general, the largest leaf area indices are recorded in July and June and the smallest in December and January. The coniferous forest shows the smallest decrease in winter.

#### 2.4. Calibration and Error Measures

The goal of a model calibration is to determine unknown parameters by adapting the calculation result to observed conditions by varying these parameters. Basically, there are two options: an automated (e.g., Latin Hypercube Sampling) and a manual calibration procedure. In automatic calibration, parameters are adjusted automatically according to a predefined search scheme and numerical measures of the goodness of fit [26]. Within this framework, a large number of parameter combinations must be generated and tested; depending on the number of parameters to be calibrated, several hundred to thousands of simulation runs are necessary. The procedure is often used for either single events or comparatively less complex models with a short runtime (see [26,27]). With long simulation durations (in this study, ~3 h for 20 months) and a large number of model parameters, automatic calibration is only of limited use. Especially for physically based models, a specific manual calibration can ensure that physically reasonable parameter combinations and value ranges are maintained. This is especially important if the detected parameter combinations are to be transferred to further similar but unobserved areas. Therefore, the manual calibration approach was chosen. In a first step, the sensitivities of all model parameters were tested with regard to their effect on stream flow. This was done by a graphical evaluation of the flow hydrographs. In a next step, the detected sensitive parameters were modified so that the difference

between the calculated values from the measured values became minimal. In the process, only one model parameter per simulation run was varied within its plausible limits. The goodness of fit of the model was assessed using the error measures and performance criteria in Table 2.

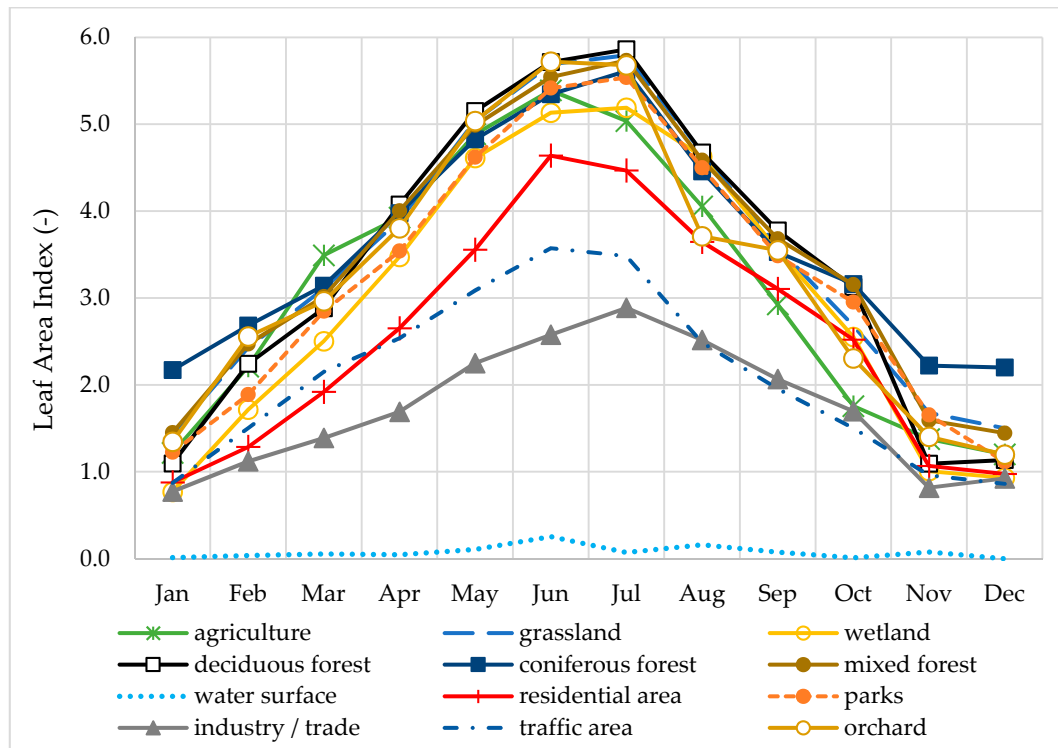


Figure 6. Average leaf area index per month derived from satellite data for different land use classes (based on one cloudless satellite image per month from November 2013 till October 2015).

Table 2. Error measures and performance criteria.

Designation	Abbreviated Designation	Formula	No.
Volume Error	$E_{Vol}$	$E_{Vol} = 1 - \frac{\int Q_{calc} dt}{\int Q_{obs} dt}$	(25)
Mean absolute Error	MAE	$MAE =  \bar{E}  = \frac{\sum_i  Obs_{i,t} - Calc_{i,t} }{n}$	(26)
Correlation Coefficient	R	$R = \frac{\sum_t (Calc_{i,t} - \overline{Calc_{i,t}}) \times (Obs_{i,t} - \overline{Obs_{i,t}})}{\sqrt{\sum_t (Calc_{i,t} - \overline{Calc_{i,t}})^2 \times \sum_t (Obs_{i,t} - \overline{Obs_{i,t}})^2}}$	(27)
Nash Sutcliffe Efficiency	NSE	$NSE = 1 - \frac{\sum_t (Obs_{i,t} - Calc_{i,t})^2}{\sum_t (Obs_{i,t} - \overline{Obs_{i,t}})^2}$	(28)

$Q_{calc}$  = calculated flow,  $Q_{obs}$  = observed flow;  $obs$  = measured value (observed);  $calc$  = calculated value; Indices:  $i$  = location,  $t$  = time,  $n$  = number of measurement data.

The volume error quantifies the total deviation in the period under consideration. The MAE indicates to what extent the simulated values deviate on average from the measured values while having the same units as the model output. R and NSE allow statements to be made about the adaption of the dynamics of the simulated flows, whereby the former tests the linear correlation and the latter allows an assessment of how well the simulated values agree with the measured ones. The disadvantage of the NSE is that it is very sensitive to outliers due to the squared differences between measured and simulated values [28]. The following table (Table 3) provides a classification to assess the goodness of fit for R and NSE.

**Table 3.** Assessment of the evaluation criteria *R* and *NSE*.

	Very Good	Good	Satisfactory	Not Satisfactory	Source
<i>R</i>	$R \geq 0.93$	$0.8 \leq R < 0.93$	$0.6 \leq R < 0.8$	$R < 0.6$	[29]
<i>NSE</i>	$>0.80$	$0.60 \leq NSE \leq 0.80$	$0.50 < NSE < 0.60$	$\leq 0.50$	[30]

### 3. Results and Discussion

#### 3.1. Sensitivity Analyses

The following table shows the parameters with the highest sensitivity to stream flow and the effects of parameter changes. Parameters not listed in Table 4, such as soil properties or the degree of sealing, have a sensitive effect on stream flow, too. However, since they were derived from soil maps or satellite data, respectively, they vary widely in space and were considered to be fixed in the process of calibration.

Initial values for the vegetation coefficients were determined according to [13]. Since they depend on local climate conditions [31], they were slightly varied and adjusted in the calibration process to achieve the best simulation results (Table 5).

**Table 4.** Parameter sensitivities and effects of parameter changes regarding stream flow (\* only SWMM-UrbanEVA).

Parameter	Unit	Calibrated Value, Range, or Calculation Formula	Sensitivity to Stream Flow	Effects of Parameter Changes/Comment
<b>Subcatchment Characteristics</b>				
Width	m	$\frac{\sqrt{Area}}{6}$	medium	The greater the width of the subcatchments, the shorter the flow path, the earlier and larger the direct peak runoff
Manning value impervious	$s (m^{1/3})^{-1}$	0.05	medium	large values slow down surface runoff and reduce peak flow
Detention storage impervious	mm	0.5	medium	Cuts peak runoff; small rain events are “swallowed” if value is too high
<b>LID Control</b>				
average LAI *	$m m^{-1}$	1.7–3.6	medium	The higher the value, the more ET, the less GW base flow in the stream
LAI monthly coefficients * (pattern)	-	0.2–1.7	medium	increases seasonal dynamics of actual ET throughout the year; Increased ET in summer leads to lower GW levels and therefore less GW inflow to stream
crop factor * ( $K_C$ )	-	0.7–1.5	high	The higher the value, the more ET, the lower the GW level, the less GW base flow in the stream
<b>Groundwater (Physical Parameters)</b>				
Porosity	-	0.43	high	Increasing the value causes delay of GW peak discharge; more extreme course of the base flows in the stream (high flows higher, lower flows lower)
Conductivity Slope	-	18	medium	the higher the value, the later the lateral GW discharges react (delay of GW peak flows)
Upper Evaporation Fraction	-	0.1	high	the lower the value, the higher the base flow in average; positive correlation with lower GW loss rate
Lower GW Loss Rate (Seep)	$mmh^{-1}$	$5.0 \times 10^{-6}$	high	the lower the value, the higher the base flow in average

Table 4. Cont.

Parameter	Unit	Calibrated Value, Range, or Calculation Formula	Sensitivity to Stream Flow	Effects of Parameter Changes/Comment
<b>Groundwater Flow Editor</b>				
A1	-	0.04 (0.0003 for sealed areas)	high	The smaller the value, the flatter/slower the flows decrease, making base flows higher
B1	-	2	high	The smaller the value, the larger the peaks, less base runoff
A2 and A3 B2	-	0 1	high	Level of surface water does not significantly affect GW flow; by setting the coefficients to zero and B2 to 1, it is excluded from the power function
Threshold Water Table Elevation	m	1.2 m below surface height	high	the lower the threshold, the higher the lateral GW discharges to the stream

Table 5. Final vegetation coefficients of the different land use classes.

Land Use Class	Crop Factor $K_C$ (-)
agriculture	1.5
wetland	1.3
grassland	1.3
industry/trade	0.7
deciduous forest	0.8
mixed forest	0.8
coniferous forest	0.8
orchard	1
residential area	0.7
parks	1.3
traffic area	0.7
water surface	0.7

The parameters under the heading “subcatchment characteristics” influence the peak height of the direct runoff while the other parameters have a direct or indirect effect on the GW level and thus on the GW inflows to the stream. Here, the role of ET under the heading “LID Controls” in Table 4 should be emphasized, as it affects the amount of deep percolating water. In particular, the LAI monthly coefficients together with the average LAI enable an intensified ET in summer (June + July, see Figure 6) controlled by the LAI and a reduced ET in winter as well as a transition phase in spring and autumn, respectively. The crop factor  $K_c$  is highly sensitive.  $K_c > 1$  increases and  $K_c < 1$  decreases ET compared to the input grass reference ET. LAI and  $K_c$  form the key parameters for influencing the annual cycle of base flows in the stream.

### 3.2. Calibration Results

Figure 7 shows the simulated hydrographs with SWMM and SWMM-UrbanEVA and the observed stream flows at the monitoring station. Accordingly, Table 6 expresses the model fit in numbers by error measures and performance criteria.

The measured and as well the simulated graphs show that the stream flow is composed of direct runoff peak flows and a base flow component. The direct runoff peak discharges strongly depend on the intensity of the input precipitation, which can vary locally, especially during heavy rainfall events. Therefore, it is important to mention that the input precipitation was not measured directly in the model area but about 8 km south of it. However, in contrast to individual rain events, it is assumed that the long-time sums of precipitation in the model area are the same as at the measuring station.

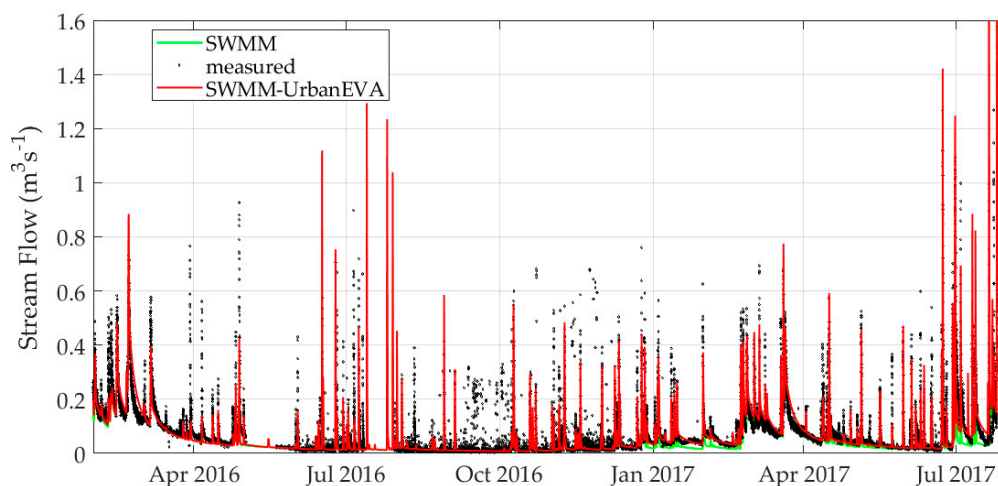


**Figure 7.** Simulated stream flow with SWMM and SWMM-UrbanEVA and observed flow at the measurement station AB.

**Table 6.** Model performance based on error measures and performance criteria related to the total flow rate in the period 21 January 2016 to 31 July 2017.

	<i>E_Vol</i> (%)	<i>MAE</i> ( $\text{m}^3\text{s}^{-1}$ )	<i>R</i> (-)	<i>NSE</i> (-)
SWMM	10.4	0.032	0.80	0.44
SWMM-UrbanEVA	3.6	0.026	0.82	0.68

The volume error of the total stream flow calculated with SWMM is quite low but decreases even more with SWMM-UrbanEVA. The same applies to the *MAE*. The *R* and *NSE* of the SWMM-UrbanEVA results indicate a good fit; in contrast to this, the total results obtained from the original SWMM version are worse, which is mainly reflected in the volume error and *NSE*. It should again be noted that the performance criteria are sensitive to non-matching peak flows, for example, if it has rained over the precipitation measurement station but not in the model area itself or vice versa. Since direct runoff peak flows are not significantly influenced by ET, they will not be considered further in this study. However, a model comparison based on error measures and performance criteria does not go far enough. Since evaporation has different effects in different seasons, a process-oriented consideration is necessary.

### 3.3. Water Balance

The following table (Table 7) lists important parameters of the water balance in the period from 1 December 2015 to 31 July 2017 (20 months). Continuity errors are smaller than 1%. The initial conditions and storage levels at the beginning of the simulation are the same for the SWMM and the SWMM-UrbanEVA model. The water balance variables of the subcatchments are summarized under the heading “Runoff Quantity”. It includes both the runoff of sealed areas of the subcatchments and those of the permeable areas. The latter are modelled as LID modules (bioretention cells). The direct surface runoff (95 mm in both cases) primarily comes from paved areas, since hardly any surface runoff is formed within the LID modules (<1 mm in both cases). It can be seen that the ET in SWMM-UrbanEVA is smaller than that calculated with SWMM in the period of time selected, hence the proportion of water that is passed on to the GW zone (“Infiltration Loss”) is larger. Therefore, more water is available to the GW flow, which is ultimately reflected in the GW inflow to the stream (“GW Inflow”). The latter makes up the largest volume share in the stream overall.

**Table 7.** Extract from the SWMM status report for the simulation period 1 December 2015–31 July 2017 (entire model area).

	SWMM-UrbanEVA	SWMM
<b>Runoff Quantity</b>	<b>Depth (mm)</b>	<b>Depth (mm)</b>
Total Precipitation	1162	1162
Evaporation Loss	666	715
Infiltration Loss	373	324
Surface Runoff	95	95
<b>Groundwater</b>	<b>Depth (mm)</b>	<b>Depth (mm)</b>
Infiltration	373	324
GW Flow	388	368
<b>Flow Routing</b>	<b>Volume (10<sup>6</sup> L)</b>	<b>Volume (10<sup>6</sup> L)</b>
Wet Weather Inflow	2144	2144
GW Inflow	8771	8302

Looking at the distribution of evaporation and infiltration loss within the LID modules, important differences between the two models and their different land use classes become apparent (Figure 8). With the official SWMM version, there are hardly any differences between the land use classes; the slight differences are only due to different soil types and different water availability depending on the placement in the terrain. The evaporation loss is about 900 mm while the infiltration loss is slightly more than 200 mm. In contrast, ET in SWMM-UrbanEVA varies from around 440 (water surfaces) to 990 (agricultural areas) and infiltration from 140 to 690 depending on the land use class. In addition, a strong linear relationship between ET and percolation to the GW zone can be determined in the model area, which is suggested by the correlation coefficient of 0.99. This again underlines the influence of ET on the percolation to GW and the resulting base flow component in the river.

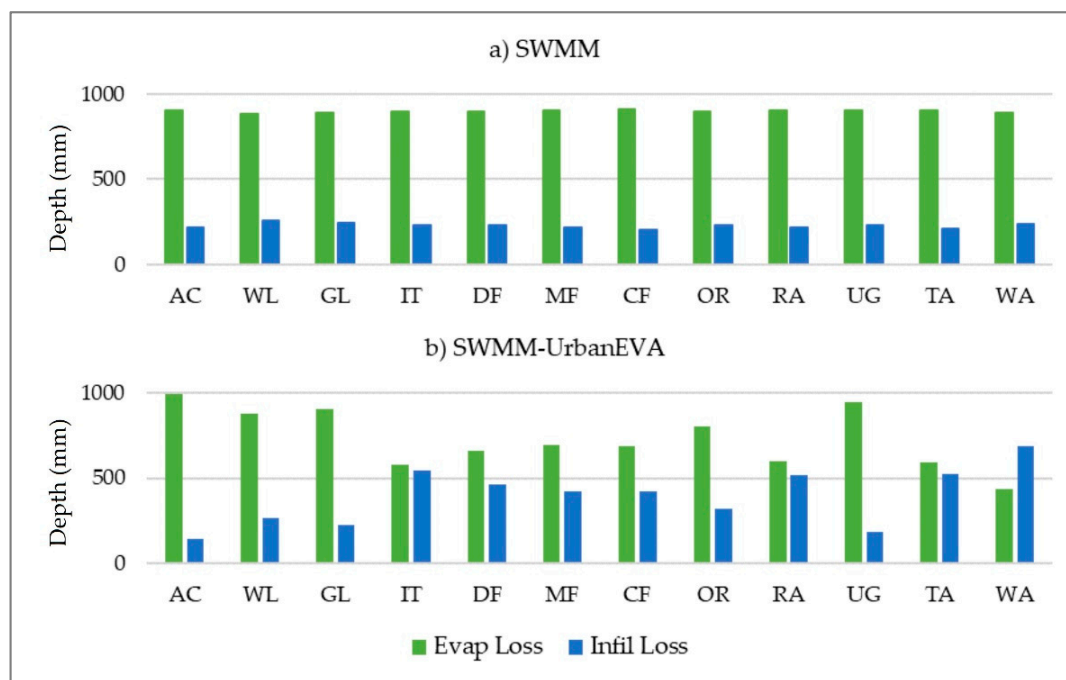


**Figure 8.** Evapotranspiration and infiltration loss in (a) the SWMM and (b) the SWMM-UrbanEVA LIDs (pervious area of a subcatchment).

### 3.4. Groundwater Table and Groundwater Flows to Stream

In the considered model area, GW inflow plays a decisive role with respect to the stream flow. These in turn depend on the GW level, more precisely on the difference between the GW level and the bottom of the receiving node of the hydraulic system, and on the values for A1 (constant) and B1 (exponent) used in the GW power function. The GW hydrographs (Figure 9) are now to be examined more closely using the example of an agricultural area and a mixed forest area.

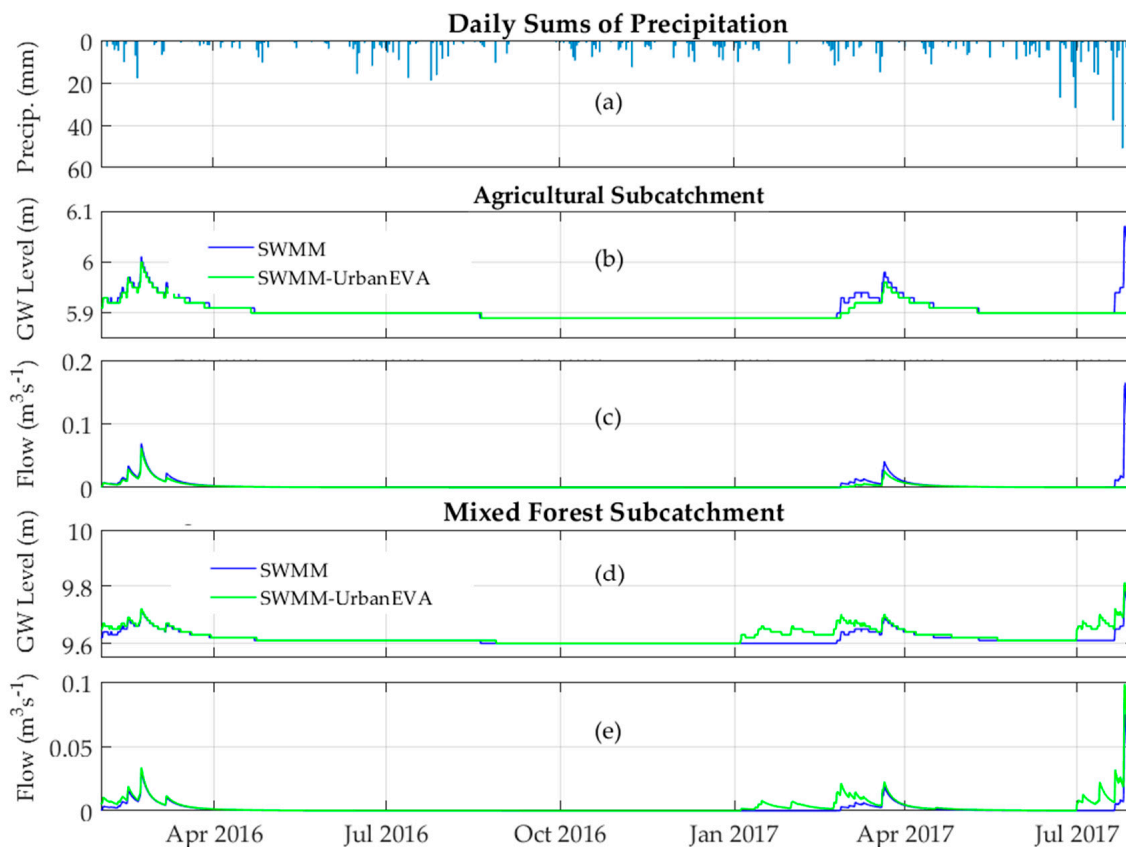


**Figure 9.** Daily sums of precipitation (a), GW flow and GW level for an agricultural subcatchment (b), (c) and for a mixed forest subcatchment (d), (e) simulated with SWMM and SWMM-UrbanEVA.

Figure 9b,c refer to an agricultural subcatchment with a crop factor of 1.5 (highest value) and a drainage threshold height of 5.89 m. In this case, the crop factor in SWMM-UrbanEVA increases the evaporation rates fundamentally and the leaf area index in turn decreases ET in winter and increases it in summer (especially in June/July). The effect under the arable land is that the GW level simulated with SWMM-UrbanEVA is slightly lower in winter and is at the threshold in a “normal” summer, such as 2016, so that no GW flow occurs. However, a significant difference between the two software versions is noticeable in wet July 2017. Due to the abundant rainfall, the GW level and flow simulated by SWMM is higher than even in winter. In SWMM-UrbanEVA, on the other hand, the precipitation is simply “swallowed” by ET so that it is not reflected in the GW level or flow.

The situation is different under a mixed forest with a crop factor of 0.8 (Figure 9d,e). Here, the GW levels and flows generated by SWMM-UrbanEVA are higher in January and February and almost identical in spring and summer—except for July 2017. In July 2017, the GW level and flow in SWMM-UrbanEVA rises already at the beginning of July and not only from the middle of the month as it is the case in the SWMM model. For the land use “forest”, the same A1 and B1 parameters were applied as under an agricultural area. It was assumed that the forest is not crossed by drainage pipes but crossed by drainage ditches. However, the very high GW peak flows suggest that a more differentiated land-use-oriented

approach to the parameters A1 and B1 would have been useful to reduce the GW flow dynamics under this forest land use class.

### 3.5. Base Flow Separation

The more water evapotranspirates, the less is available for deep seepage and GW inflow to the stream. To show the differences in base flows, a hydrograph separation was performed based on a 3-day sliding interval. Figure 10 illustrates the separated base flow hydrographs of the measured, the SWMM, and the SWMM-UrbanEVA stream flow at the observation point AB.

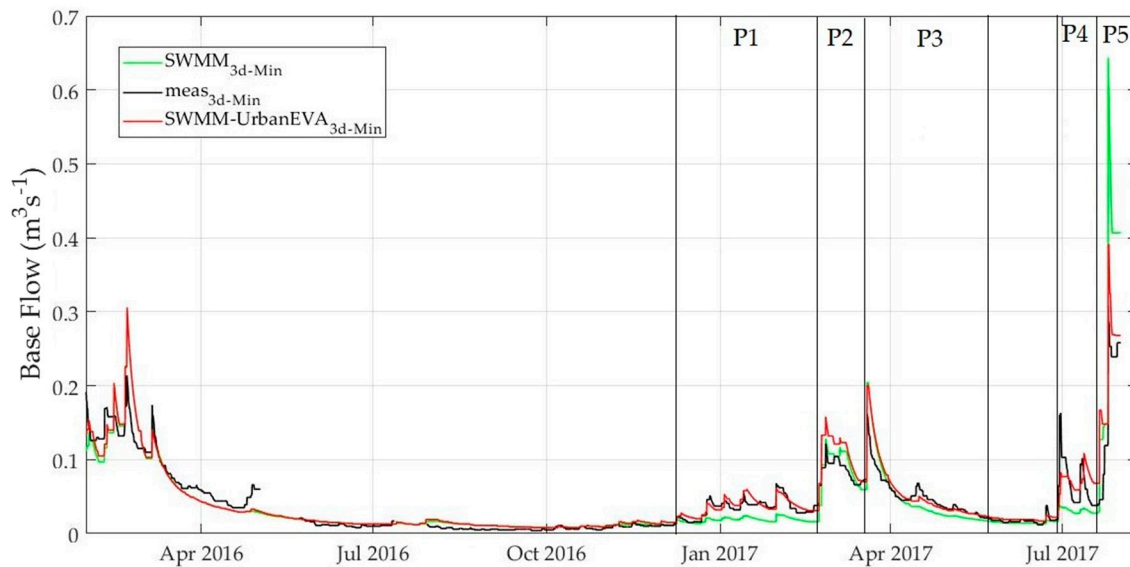


**Figure 10.** Minimum flows of a 3-day sliding interval of measured data (abbreviation “meas”), flows generated with the official SWMM version and SWMM-UrbanEVA.

In principle, the dynamics from January 2016 to mid-December 2016 in both models correspond very well with reality. The months of June to October 2016 are normally dry summer months with typically little base flow. It can be assumed that only the low-lying wetlands still contribute to base flow. At this point, it must be emphasized once again that in the model, GW only drains to the river if a fixed threshold value is exceeded. As the figure shows, the simulated base flows differ mainly from mid-December 2016 to the end of May 2017 and in July 2017. Five phases can be distinguished more precisely:

- P1: 1 December 2016–20 February 2017  
Transition phase from low to high base flows; SWMM-UrbanEVA base flows adapt very good to the measured ones, while those produced with SWMM are basically too low. Here, the evaporation in SWMM is too high since leaf fall cannot be incorporated in SWMM.
- P2: 20 February 2017–19 March 2017  
Phase of high base flows; SWMM-UrbanEVA base flows are higher than the observed ones while those generated with SWMM fit well. Here, the discrepancy can be explained by two possible reasons: According to [13], the crop factor is not constant but changes in dependence of three developmental stages with specific water demands: an initial start-up phase, an intermediate phase in which the highest crop factors (or crop coefficients) are recorded, and a final phase in which the factor decreases again. If this could be taken into account in SWMM-UrbanEVA, it would be possible to calibrate the model, especially the aquifer, differently to achieve an even better adaptation. Another reason could be incorrect leaf area indices, as these were derived from satellite data and this indirect measuring method can lead to underestimation; only spectral data



are evaluated and leaves lying on top of each other might not be considered. Besides, the spatial resolution is rather low.

- P3: 19 March 2017–31 May 2017  
Very high base flows at the beginning of the period caused by voluminous precipitation and exhausted storage capacities in the soil layer. The subsequent emptying of the storage systems is basically reproduced well by both models, but the SWMM-UrbanEVA base flows react more dynamically and therefore adapt a little better.
- P4: 1 July 2017–20 July 2017  
In this summer month, base flows are above average, due to the relatively humid previous month of June and the subsequent heavy rainfall events in July. At the same time, July is the month with the highest recorded leaf area indices. In the SWMM-UrbanEVA model, GW drainage systems start to operate as early as 1 July, in contrast to the SWMM model, which starts later. This results in a better adapted course of the SWMM-UrbanEVA base flow compared to the measured data.
- P5: 20 July 2017–31 July 2017  
In the last third of the month, in addition to the high pre-humidity, very strong rainfall occurs, which causes the GW level to rise and restart all drainage systems. In this phase, the largest deviations between SWMM-UrbanEVA and SWMM are registered. The SWMM base flows are extraordinarily high and therefore do not offer a realistic curve. The SWMM-UrbanEVA hydrograph adapts much better, but the peak value of the base flow is still too high during this period. This is probably due to wooded areas, which provide too high peak flows (see Table 8).

**Table 8.** Model performance based on error measures and performance criteria related to the base flow rate in the period 21 January 2016 to 31 July 2017.

	MAE (m <sup>3</sup> s <sup>-1</sup> )	R (-)	NSE (-)
SWMM	0.014	0.88	0.81
SWMM-UrbanEVA	0.011	0.93	0.85

If the basic flows are considered without the direct runoff peak flows, the valuation criteria improve considerably. Table 8 shows that the base flows are very well represented by the SWMM-UrbanEVA model both on average and in their dynamics. The results produced with SWMM are nevertheless in the “good” range.

#### 4. Conclusions

The present study was carried out to show the importance of ET and its influence on the base flows of a stream system in the north German lowlands. It was shown that for near natural landscapes, such as agricultural areas, the inclusion of land-use-dependent ET is indispensable for the calculation of water balances over a cross-seasonal period. However, this only applies to areas where the inflow of GW or drainage water to the stream or river plays an important role. Especially in relatively wet summer months, SWMM extremely overestimates the GW inflow because the stocks do not evapotranspire enough rainwater.

In contrast to the original SWMM version, SWMM-UrbanEVA makes it possible to distinguish between different land use classes and their specific water demands, which is particularly important in small catchments, where the respective characteristics are more pronounced.

A suggestion for improvement can still be made here: Since the water demands of a plant behave differently in different growth stages, it would be useful to allow the input of a dynamic crop factor to achieve an even better adaptation. Nevertheless, single precipitation events (scenarios) can be calculated with SWMM as well as with SWMM-UrbanEVA since ET does not affect direct runoff peaks.

Summarizing, SWMM-UrbanEVA introduces a significant improvement towards process-oriented water balance modelling. However, the introduced additional processes (transpiration, interception,

and evaporation) account for computation time. For the presented model area with its 626 subcatchments, 590 junction nodes, and 580 conduit links (including Rainfall-Runoff, Horton Infiltration, GW Flow, and dynamic wave flow routing), SWMM-UrbanEVA requires 2 h 50 min for 20 months, while SWMM requires only 20 min. The ratio is 1:8.5. The computing time of SWMM-UrbanEVA is approximately the same as that of comparable software (e.g., MIKE-SHE).

However, the ability to integrate urban drainage systems and near natural river basins in one single model puts the increased computing time in a different perspective. In other model environments, integrated modelling would require numeric coupling of different modules, often connected with serious numeric stability problems.

**Author Contributions:** Conceptualization, F.K.; methodology, F.K. and J.T.; validation, F.K.; formal analysis, F.K.; investigation, F.K.; resources, F.K.; data curation, F.K.; writing—original draft preparation, F.K.; writing—review and editing, J.T.; visualization, F.K.; supervision, J.T.; project administration, J.T.; funding acquisition, J.T. All authors have read and agreed to the published version of the manuscript.

**Funding:** This study was conducted within the framework of the Project PROSPER-RO, funded by BMBF, grant number 033L212. We acknowledge financial support by Deutsche Forschungsgemeinschaft and Universität Rostock within the funding program Open Access Publishing.

**Acknowledgments:** We thank Birgitta Hörnschemeyer, Malte Henrichs and Mathias Uhl from IWARU, University of Applied Sciences Münster, for developing and providing the software SWMM-UrbanEVA as well as for the good introduction to the tool.

**Conflicts of Interest:** The authors declare no conflict of interest. The funders had no role in the design of the study; in the collection, analyses, or interpretation of data; in the writing of the manuscript, or in the decision to publish the results.

## References

- Rossman, L. Storm Water Management Model: User's Manual Version 5.1. EPA/600/R-14/413 (NTIS EPA/600/R-14/413b). Available online: [https://www.epa.gov/sites/production/files/2019-02/documents/epaswmm5\\_1\\_manual\\_master\\_8-2-15.pdf](https://www.epa.gov/sites/production/files/2019-02/documents/epaswmm5_1_manual_master_8-2-15.pdf) (accessed on 29 June 2020).
- Hydrologic Engineering Center. *Hydrologic Modeling System HEC-HMS Technical Reference Manual*; United States Army Corps of Engineers: Washington, DC, USA, 2000. Available online: [https://www.hec.usace.army.mil/software/hec-hms/documentation/HECHMS\\_Technical%20Reference%20Manual\\_\(CPD-74B\).pdf](https://www.hec.usace.army.mil/software/hec-hms/documentation/HECHMS_Technical%20Reference%20Manual_(CPD-74B).pdf) (accessed on 26 October 2020).
- Moynihhan, K.; Vasconcelos, J. SWMM modeling of a rural watershed in the lower coastal plains of the United States. *J. Water Manag. Model.* **2014**. [CrossRef]
- Davis, J.P.; Rohrer, C.A.; Roesner, L.A. Calibration of rural watershed models in the North Carolina Piedmont Ecoregion. In Proceedings of the World Environmental and Water Resources Congress 2007. Available online: <https://ascelibrary.org/doi/10.1061/40927%28243%29574> (accessed on 22 October 2020).
- Talbot, M.; McGuire, O.; Olivier, C.; Fleming, R. Parameterization and application of agricultural best management practices in a rural Ontario watershed using PCSWMM. *J. Water Manag. Model.* **2016**. [CrossRef]
- Pretorius, H.; James, W.; Smit, J. A Strategy for managing deficiencies of SWMM modeling for large undeveloped semi-arid watersheds. *J. Water Manag. Model.* **2013**. [CrossRef]
- Tsai, L.-Y.; Chen, C.-F.; Fan, C.-H.; Lin, J.-Y. Using the HSPF and SWMM Models in a High Pervious Watershed and Estimating Their Parameter Sensitivity. *Water* **2017**, *9*, 780. [CrossRef]
- Tu, M.-C.; Wadzuk, B.; Traver, R. Methodology to simulate unsaturated zone hydrology in storm water management model (SWMM) for green infrastructure design and evaluation. *PLoS ONE* **2020**, *15*, e0235528. [CrossRef] [PubMed]
- Feng, Y.; Burian, S. Improving evapotranspiration mechanisms in the U.S. Environmental Protection Agency's storm water management model. *J. Hydrol. Eng.* **2016**, *21*, 6016007. [CrossRef]
- Hörnschemeyer, B.; Henrichs, M.; Uhl, M. Setting up a SWMM-integrated model for the evapotranspiration of urban vegetation. In Proceedings of the NOVATECH Lyon 2019, Lyon, France, 1–5 July 2019; pp. 1–4.
- Hörnschemeyer, B. *Modellierung der Verdunstung Urbaner Vegetation: Weiterentwicklung des LID-Bausteins im US EPA Storm Water Management Model*; Springer Spektrum: Berlin, Germany, 2019; p. 197.

12. Hörschemeyer, B.; Henrichs, M.; Uhl, M. Ein SWMM-Baustein für die Berechnung der Evapotranspiration von urbaner Vegetation. In Proceedings of the Aqua Urbanica 2019: Regenwasser Weiterdenken—Bemessen trifft Gestalten, Rigi Kaltbad, Switzerland, 8–10 September 2019; pp. 133–140.
13. Allan, R.; Pereira, L.; Raes, D.; Smith, M. FAO Irrigation and Drainage Paper No. 56. Available online: <http://www.fao.org/3/X0490E/x0490e00.htm> (accessed on 24 September 2020).
14. Hydrologischer Atlas Deutschland. Teil 2: Hydrometeorologie; Bundesamt für Gewässerkunde (BfG). Available online: <https://geoportal.bafg.de/mapapps/resources/apps/HAD/index.html?lang=de> (accessed on 24 September 2020).
15. Pettyjohn, W.A.; Henning, R. *Preliminary estimate of ground-water recharge rates, related streamflow and water quality in Ohio: Ohio State University Water Resources Center Project Completion*; The Ohio State University: Columbus, OH, USA, 1979.
16. Rossman, L.; Huber, W. Storm Water Management Model: Reference Manual Volume I—Hydrology (Revised). EPA/600/R-15/162A. Available online: <https://nepis.epa.gov/Exe/ZyPDF.cgi?P100NYRA.PDF?Dockey=P100NYRA.PDF> (accessed on 24 September 2020).
17. Hossain, S.; Hewa, G.A.; Wella-Hewage, S. A Comparison of continuous and event-based rainfall–runoff (RR) modelling using EPA-SWMM. *Water* **2019**, *11*, 611. [[CrossRef](#)]
18. Rossman, L. Storm Water Management Model: Reference Manual Volume II—Hydraulics. EPA/600/R-17/111. Available online: <https://nepis.epa.gov/Exe/ZyPDF.cgi?Dockey=P100S9AS.pdf> (accessed on 24 September 2020).
19. Bremicker, M. Aufbau eines Wasserhaushaltsmodells für das Weser- und das Ostsee-Einzugsgebiet als Baustein eines Atmosphären-Hydrologie-Modells. Ph.D. Thesis, Albert-Ludwigs-Universität Freiburg, Freiburg, Germany, 1998.
20. Bremicker, M. Das Wasserhaushaltsmodell LARSIM: Modellgrundlagen und Anwendungsbeispiele. *Freibg. Schr. Hydrol.* **2000**, *11*, 1–130.
21. Braden, H. Ein Energiehaushalts- und Verdunstungsmodell für Wasser und Stoffhaushaltsuntersuchungen landwirtschaftlich genutzter Einzugsgebiete. *Mitt. Dtsch. Bodenkd. Ges.* **1985**, *42*, 294–299.
22. Deardorff, J.W. Efficient prediction of ground surface temperature and moisture, with inclusion of a layer of vegetation. *J. Geophys. Res.* **1978**, *83*, 1889–1903. [[CrossRef](#)]
23. Dickinson, R.E. *Modeling Evapotranspiration for Three-Dimensional Global Climate Models*; Geophysical Monograph Series; AGU Publishing: Washington, DC, USA, 1984; ISBN 9781118666036. [[CrossRef](#)]
24. Kroes, J.G.; van Dam, J.C.; Groenendijk, P.; Hendriks, R.F.A.; Jacobs, C.M.J. *SWAP Version 3.2—Theory Description and User Manual*; Alterra Wageningen: Wageningen, The Netherlands, 2008.
25. Schulla, J. *Model Description WaSiM (Water Balance Simulation Model)*; Hydrology Software Consulting: Zürich, Switzerland, 2012.
26. Madsen, H. Automatic calibration of a conceptual rainfall–runoff model using multiple objectives. *J. Hydrol.* **2000**, *235*, 276–288. [[CrossRef](#)]
27. Barco, J.; Wong, K.M.; Stenstrom, M.K. Automatic Calibration of the U.S. EPA SWMM Model for a Large Urban Catchment. *J. Hydraul. Eng.* **2008**, *134*, 466–474. [[CrossRef](#)]
28. Krause, P.; Boyle, D.; Bäse, F. Comparison of different efficiency criteria for hydrological model assessment. *Adv. Geosci.* **2005**, *5*, 89–97. [[CrossRef](#)]
29. Chiew, F.H.; McMahon, T.A. Assessing the adequacy of catchment streamflow yield estimates. *Aust. J. Soil Res.* **1993**, *31*, 665–680. [[CrossRef](#)]
30. Moriasi, D.; Gitau, M.; Pai, N.; Daggupati, P. Hydrologic and water quality models: Performance measures and evaluation criteria. *Trans. ASABE* **2015**, *58*, 1763–1785. [[CrossRef](#)]
31. Zenker, T. Verdunstungswiderstände und Gras-Referenzverdunstung: Lysimeteruntersuchungen zum Penman-Monteith-Ansatz im Berliner Raum. Ph.D. Thesis, Technische Universität Berlin, ehemalige Fakultät VII—Architektur Umwelt Gesellschaft, Berlin, Germany, January 2003.

**Publisher’s Note:** MDPI stays neutral with regard to jurisdictional claims in published maps and institutional affiliations.



© 2020 by the authors. Licensee MDPI, Basel, Switzerland. This article is an open access article distributed under the terms and conditions of the Creative Commons Attribution (CC BY) license (<http://creativecommons.org/licenses/by/4.0/>).